ADVANCED MATERIALS
www.advmat.de

Reverse-Offset Printed Ultrathin Ag Mesh for Robust Conformal Transparent Electrodes for High-Performance Organic Photovoltaics

Zhi Jiang, Kenjiro Fukuda, Xiaomin Xu, Sungjun Park, Daishi Inoue, Hanbit Jin, Masahiko Saito, Itaru Osaka, Kazuo Takimiya, and Takao Someya**

Mechanically durable transparent electrodes are needed in flexible optoelectronic devices to realize their long-term stable functioning, for applications in various fields such as energy, healthcare, and soft robotics. Several promising transparent electrodes based on nanomaterials have been previously reported to replace the conventional and fragile indium-tin oxide (ITO); however, obtaining feasible printed transparent electrodes for ultraflexible devices with a multistack structure is still a great challenge. Here, a printed ultrathin (uniform thickness of 100 nm) Ag mesh transparent electrode is demonstrated, simultaneously achieving high conductance, high transparency, and good mechanical properties. It shows a 17 Ω sq^{-1} sheet resistance (R_{sh}) with 93.2% transmittance, which surpasses the performance of sputtered ITO electrodes and other ultrathin Ag mesh transparent electrodes. The conductance is stable after 500 cycles of 100% stretch/release deformation, with an insignificant increase (10.6%) in R_{sh} by adopting a buckling structure. Furthermore, organic photovoltaics (OPVs) using our Ag mesh transparent electrodes achieve a power conversion efficiency of 8.3%, which is comparable to the performance of ITO-based OPVs.

Conformable large-area optoelectronic devices are necessary for future applications in sensing,[1] imaging,[2] energy-harvesting,[3,4] healthcare,[5] and robotics[6] that require integration onto three-dimensionally curved surfaces. Transparent conductors are indispensable to those photonic devices for their unique optical and electrical properties. Indium-tin oxide (ITO) electrodes are the predominant candidates for rigid photonic devices due to their dual benefits of offering high conductivity and transparency (around 10 Ω sq^{-1} at 90% transmittance).[3,7,8]

In order to improve the flexibility of optoelectronic devices, mechanically durable transparent electrodes, which are derived from nanomaterials and exhibit comparable/higher conductivity and transparency with/than those of ITO, have been intensively studied.[9] A state-of-the-art transparent electrode (fabricated by electrospinning and thermal evaporation) based on networks consisting of vertically interlaced mesoscale Cu wires and Au nanowires reported a 0.36 Ω sq^{-1} sheet resistance (R_{sh}) at 92% transmittance.[10] ITO-free electrodes typically have flexibility and bendability with a millimeter-scale bending radius, and their conductance decreases sharply when highly stretched due to the fatigue of metallic network film.[11–13] Structural design approaches have been used to further improve their mechanical properties. For example, a pre-strained Au nanofiber network film with a serpentine morphology showed good stretchability (to 150% strain) and mechanical stability (large strain for 10 000 cycles without obvious fatigue).[14]

Nanomaterial-based transparent electrodes can potentially be fabricated by printing processes, which is highly desirable due to their fabrication characters featuring large area and high throughput.[15] Printed transparent electrodes are expected to simultaneously achieve high conductance, high transparency, and ultrathinness. Ag nanoparticle inks are the most popular choice for such transparent electrodes with freely designed

Z. Jiang, Dr. K. Fukuda, Prof. T. Someya
Thin-Film Device Laboratory
RIKEN
2-1 Hirosawa, Wako, Saitama 351-0198, Japan
E-mail: kenjiro.fukuda@riken.jp; takao.someya@riken.jp

Z. Jiang, H. Jin, Prof. T. Someya
Electrical and Electronic Engineering and Information Systems
The University of Tokyo
7-3-1 Bunkyo-ku, Tokyo 113-8656, Japan

The ORCID identification number(s) for the author(s) of this article can be found under https://doi.org/10.1002/adma.201707526.

DOI: 10.1002/adma.201707526

Dr. K. Fukuda, Dr. X. Xu, Dr. S. Park, Dr. D. Inoue, Prof. K. Takimiya, Prof. T. Someya
Center for Emergent Matter Science
RIKEN
2-1 Hirosawa, Wako, Saitama 351-0198, Japan

Dr. K. Fukuda
Japan Science and Technology Agency
PRESTO
4-1-8 Honcho, Kawaguchi, Saitama 332-0012, Japan

Dr. M. Saito, Prof. I. Osaka
Department of Applied Chemistry
Hiroshima University
1-4-1 Kagamiyama, Higashi-Hiroshima, Hiroshima 739-8527, Japan

patterns.[16] The highest previously reported performance of printed Ag mesh transparent electrodes was 2 Ω sq^{-1} R_{sh} at 89.7% transmittance with a film thickness more than 2 µm, which was enabled by embedding the mesh structure in thick substrates.[17] The total thickness of these transparent electrodes is more than hundreds of micrometers, so that the flexibility and conformability of devices is limited with millimeter-scale bending radius.[11,16] Reducing the thickness of mesh structures (to less than 100 nm) on ultrathin flat substrates (1 µm) is necessary for ultraflexible optoelectronics with multistack structures. Printed ultrathin mesh structures (around 100 nm) were previously reported by ink-jet printing (95 µm in width),[18] showing a 4 Ω sq^{-1} R_{sh} at 75% transmittance. Further line width reduction can improve the transmittance, and keeping a uniform thickness over a large area is important to achieve high conductance with good reproducibility.[19] Recently, reverse-offset printed Ag mesh structures (0.3 µm thick and 3 µm width) were fabricated on 180 µm thick polycarbonate substrates, showing a 27 Ω sq^{-1} R_{sh} at 85% transmittance.[20]

However, fabricating printed Ag mesh transparent electrodes that simultaneously achieve high conductance, ultrathinness, and good mechanical durability remains challenging. The major obstacle is caused by the trade-off between the thickness and the conductance, as well as the mechanical properties of mesh structures. Highly conductive printed Ag mesh films usually have a thickness in the range of 2–20 µm, which can limit the flexibility and inhibit utilization in ultrathin photonic devices.[21] Reducing the thickness (to less than 100 nm) of mesh structures is necessary, and keeping a good uniformity on a large area with high printing resolution is critical to retain a high conductance at a high transparency, which has not been achieved when the thickness is downscaled around 100 nm or less. In addition, ultraflexible substrates are needed for the adoption of a buckling structure to achieve a good stretchability and durability, which has not been reported in ITO-free printed transparent electrodes.

Here we show printed transparent electrodes that simultaneously achieve high conductivity, ultrathinness, and excellent mechanical durability. Ag mesh structures with narrow line width (5 µm), ultrathinness (100 nm), and good thickness uniformity can be patterned by a reverse-offset printing technology on ultraflexible substrates (1 µm). The Ag mesh electrodes offer high conductivity and transparency, i.e., 17 Ω sq^{-1} R_{sh} at 93.2% transmittance, which surpasses the performance of sputtered ITO on ultraflexible substrates and other previously reported ultrathin Ag mesh transparent electrodes.[11,16,22–24] Moreover, by adopting a buckling structure, they demonstrated superior mechanical stability, displaying only a 16.6% increase in R_{sh} under 50% compression and a 10.6% increase in R_{sh} after 500 stretch/release cycles at 100% strain. Due to the above features, this Ag mesh transparent electrode can be easily integrated in ultrathin photonic devices. To show the feasibility of the printed electrodes, ultrathin organic photovoltaic devices were fabricated with the Ag mesh transparent electrodes. The organic photovoltaics (OPVs) exhibited an average power conversion efficiency (PCE) value of 8.3% and a high yield of more than 90%, which are the highest among OPVs with Ag mesh electrodes and comparable to OPVs with ITO electrodes.

Our Ag mesh transparent electrodes were fabricated by a reverse-offset printing method, featuring high-efficiency, high-throughput, arbitrary patterning, and high resolution. The fabrication procedure and details are given in **Figure 1**a and in the Device Fabrication section in the Supporting Information. Notably, Ag mesh electrodes with freely designed patterns (Figure S1a,b, Supporting Information) can be obtained directly, which is a desirable aspect for optoelectronics because high-resolution patterning and precise alignment among several layers is necessary for such devices.[25] The speed of our printing process was ≈112.5 mm min^{-1} in the plane direction and highly efficient compared to other printing techniques such as ink-jet printing,[26] electron beam lithography,[22] nanoimprint,[23] and direct laser writing on printed film.[24]

Another merit of this reverse-offset printing process is its high resolution. Here, we demonstrate that the resolution for printed lines can be downscaled to as small as 5 µm (smaller than those by other reported techniques,[22–24,26] i.e., 12 µm on flat substrates). For our design, a 5 µm wide Ag square mesh (Figure 1b) was used as the smallest space length (Figure S2a–d, Supporting Information). In addition, the printed ultrathin Ag mesh (100 nm) has a good line edge straightness and thickness uniformity over a large area (Figure 1c,d), which has not been achieved in other printed Ag mesh electrodes or solution-processed nanowire/nanofiber based transparent electrodes.[10,27–30] Owing to the above features, it can be easily utilized as a transparent electrode for ultrathin photonic devices with multistack structures.

Considering the influence of sintering temperature on the water contact angle and its impact on the work function (Figure S3, Supporting Information), a sintering post-treatment at 210 °C for 2 h was chosen for the Ag mesh due to its good wetting within the heat tolerance range of the polyimide substrate and its suitable work function of around 4.85 eV. Ag nanoparticles were joined together after sintering (Figure S4, Supporting Information), leading to a sharp increase in the conductance of the printed electrodes.[31] The Ag mesh transparent electrodes on a 1 µm thick polyimide can be easily peeled off from the glass substrate (Figure S1c, Supporting Information). As a result, a freestanding sample displayed good conformability when attached to textiles (Figure S1d, Supporting Information).

The conformal Ag mesh transparent electrodes demonstrated higher conductance and transmittance than sputtered ITO on polymer substrates[32] and other reported ultrathin Ag mesh electrodes. The performance of the Ag mesh electrodes can be tuned by adjusting its space length between adjacent lines (**Figure 2**). By increasing the space length (corresponding optical images and UV spectra are given in Figures S5 and S6 in the Supporting Information), its conductance is gradually decreased (Figure 2a), whereas its transmittance is increased (Figure 2b). It should be noted that an Ag mesh with a space length of 95 µm has a lower optical loss (6.77%) than its theoretical coverage rate (9.75%) due to the thinness and porous structure (Figure S6, Supporting Information). Moreover, it achieved an excellent conductance at this transmittance, i.e., ≈17 Ω sq^{-1} in R_{sh}, which is one of the best performances among roll-to-roll compatible transparent electrodes (Figure 2c; Table S1, Supporting Information).[11,16,22–24]

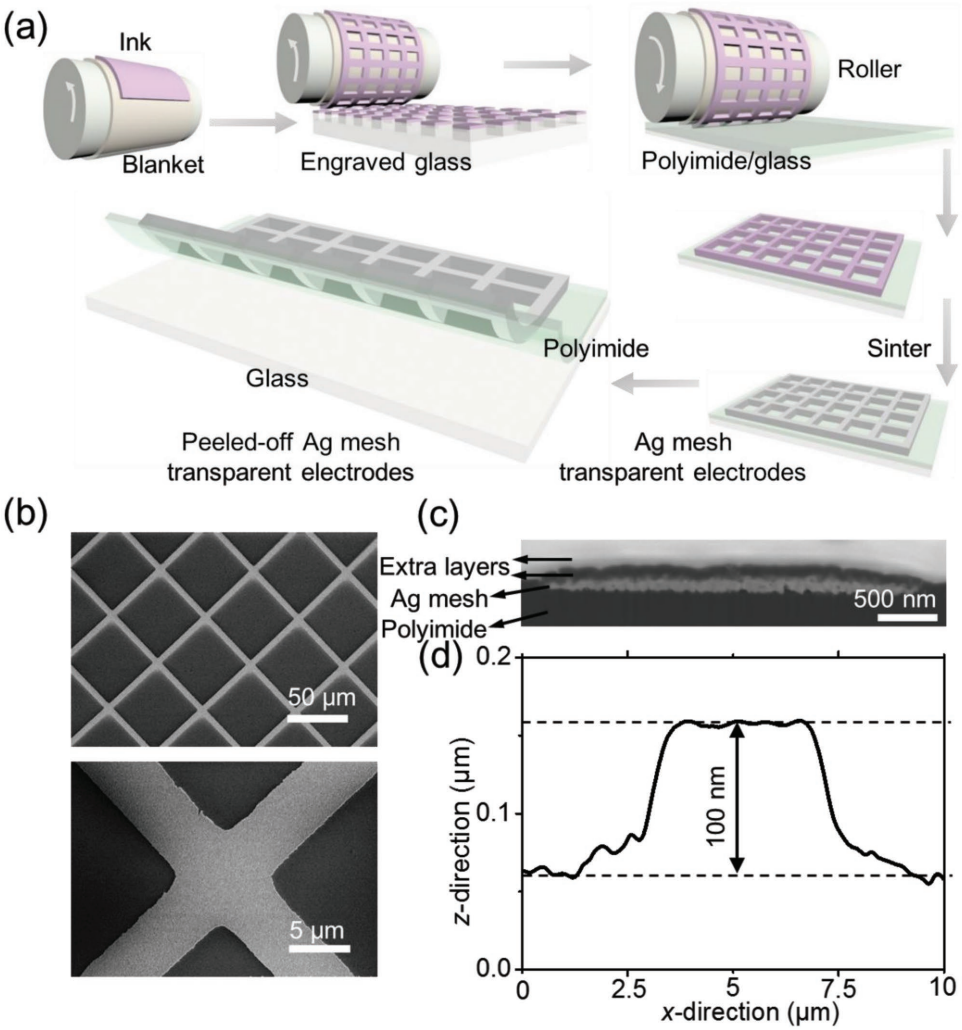

Figure 1. Ultrathin Ag mesh transparent electrodes on 1 μm thick polyimide substrate by reverse-offset printing. a) Schematic for the fabrication process of ultrathin Ag mesh transparent electrodes. b) SEM images of Ag mesh, demonstrating a space length among Ag lines of 45 μm (top) and line width of 5 μm (bottom). c) Cross-section SEM image of an Ag line, showing the good thickness uniformity and line edge straightness. (From bottom to top, there are four layers, corresponding to polyimide, Ag mesh, and other two conductive layers for preparing cross-section samples, respectively.) d) Surface profile measurement on an Ag mesh line, showing a thickness of around 100 nm.

For the application of this Ag mesh transparent electrode in OPVs, an O_2 plasma treatment was needed to create a high-quality $ZnAc_2$ layer; however, this processing step can also degrade the conductivity of the Ag mesh electrodes (Figure S7, Supporting Information) due to the oxidation of the metal. Surprisingly, its conductance was recovered by forming a ZnO layer via thermal baking due to the redox reaction[33] and/or self-decomposition of Ag_2O.[34]

As a stretchable conductor, this ultrathin Ag mesh transparent electrode showed good mechanical properties, including good adhesion to substrates, strong mechanical robustness, and excellent stability. The details of the adhesion test can be found in the Device Characterization section in the Supporting Information. The conductance of the Ag mesh transparent electrode was stable after 20 peeling tests by 3M polyimide tape (Figure S8, Supporting Information), indicating good adhesion between the Ag mesh and the polyimide substrates. One possible reason for such good adhesion is the existence of amino groups on polyimide,[35] which can bond to Ag nanoparticles.[36]

The setup for the mechanical testing is shown in **Figure 3**a, and the details can be found in the Device Characterization section in the Supporting Information. Figure 3b shows a comparison of the optical images of the Ag mesh electrodes under 0% and 50% compression. Due to the good conformability enabled by the ultrathinness, Ag mesh electrodes formed a buckling structure with the elastomer, and the minimum bending radius reached less than 10 μm (Figure S9, Supporting Information), which is the smallest bending radius reported for ITO-free transparent electrodes.

As for the Ag mesh electrode's mechanical properties, R_{sh} increased only 16.6% compared with the original value under 50% compression (Figure 3c), which is far more durable than the fragile ITO electrodes that had an 885% increase in R_{sh} under the same strain. Furthermore, we also tested the electrode's stability under stretch/release cycle test, where

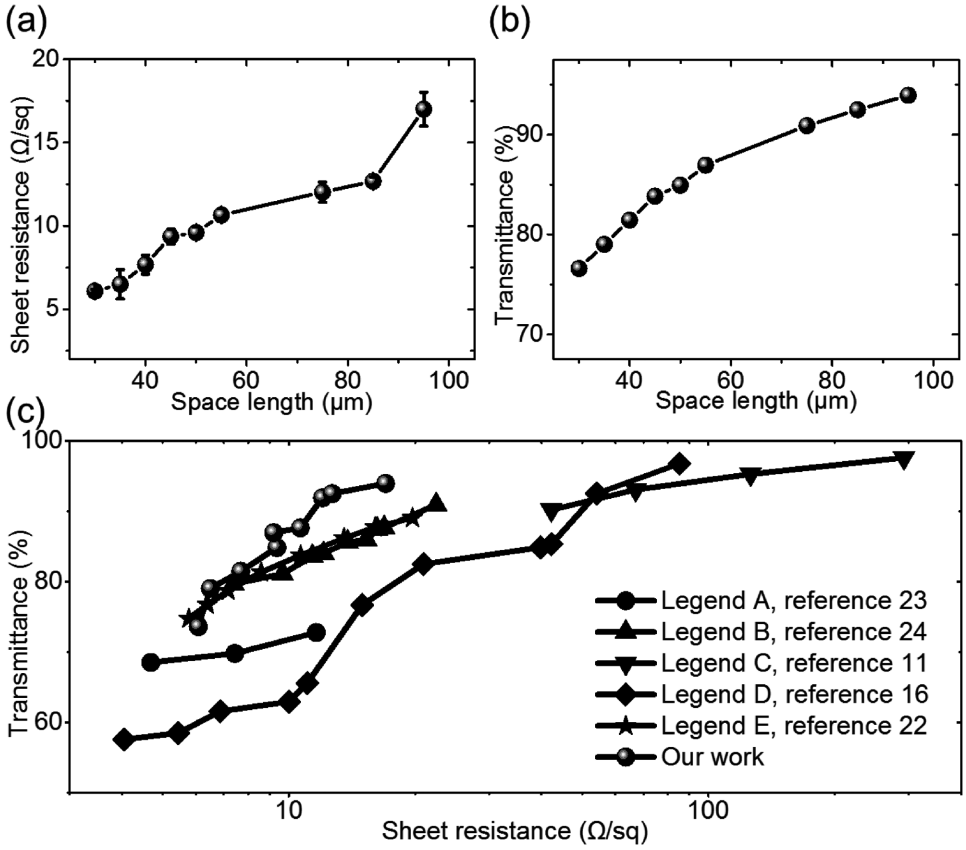

Figure 2. Performance of printed Ag mesh transparent electrodes. a) Space length versus sheet resistance. b) Space length versus transmittance (at 550 nm). c) Sheet resistance versus optical transmission (at 550 nm). The performances of graphene, silver nanowires, and printed ultrathin Ag mesh by other techniques are shown for comparison.[11,16,22–24] Note that the transmittance mentioned here does not include the transmittance of the substrate.

their stretchability was enabled by a buckling structure. The ITO electrode had a 460.9% increase in R_{sh} after 120 cycles, which also showed greatly changed R_{sh} during stretch/release deformation (up to around 2500% increase); however, after 120 cycles, the ITO electrode had failed due to severe cracking (Figure 3d; FigureS10, Supporting Information). In contrast, the Ag mesh electrodes can withstand 500 cycles with only a 10.6% increase in R_{sh} (Figure 3d). More specifically, the Ag mesh electrodes showed a stable conductance where the increase in R_{sh} was 7.6%, 8.7%, 10.0%, and 10.5% after 100, 200, 300, and 400 cycles, respectively. Figure 3e shows the Ag mesh electrode performance during the cycle test, where its conductivity showed good recovery. This behavior can be seen in the enlarged inset where the R_{sh} is shown around the 200th cycle and the 400th cycle. The insignificant increase in R_{sh} for the Ag mesh electrode most likely originated from tiny cracks formed during the cycle test (Figure S11, Supporting Information).

We fabricated ultrathin OPVs utilizing the Ag mesh/1 μm thick polyimide electrode. The fabrication details can be found in the Device Fabrication section and in Figure S12 in the Supporting Information. The total thickness of the OPV was less than 2.5 μm, including the 1 μm thick polyimide substrate and 1 μm thick parylene encapsulation layer. The structure of the OPV can be seen in **Figure 4**a. In this device, the material layers consist of the Ag mesh transparent electrode, ZnO, an active layer, PEDOT:PSS, and Ag electrode. The active layer was a blended film consisting of a thiazolothiazole–naphthobisthiadiazole copolymer (PTzNTz)[37] (Figure 4b) and [6,6]-phenyl-C_{71}-butyric acid methyl ester ($PC_{71}BM$). In order to obtain a good modification of the Ag mesh electrode's work function (Figure 4c), a complete coating of ZnO on top of the Ag mesh is critical. The ZnO layer provided the Ag mesh electrode with a smooth surface (Figure S13, Supporting Information), which in turn tuned its work function, and enabled the high yield of OPVs (more than 90%).

Next, we investigated how varying the parameters of the Ag mesh transparent electrode influenced the performance of OPVs. Figure S14a in the Supporting Information shows J–V curves of OPVs utilizing the Ag mesh transparent electrodes with the space length ranging from 35 to 75 μm. In order to provide a clear comparison, the corresponding PCE, short-circuit current (J_{SC}), open-circuit voltage (V_{OC}), and fill factor (FF) are given in Figure 4d,e, and Table S2 in the Supporting Information. It is noteworthy to mention that PCE reached a maximum value using Ag mesh electrodes with space length ranging from 45 to 50 μm. This phenomenon can be attributed to the trade-off between transmittance and the distance that light-generated electrons need to cross before reaching the cathode. In other words, smaller J_{SC} should be the result of less light passing through when space length became shorter while

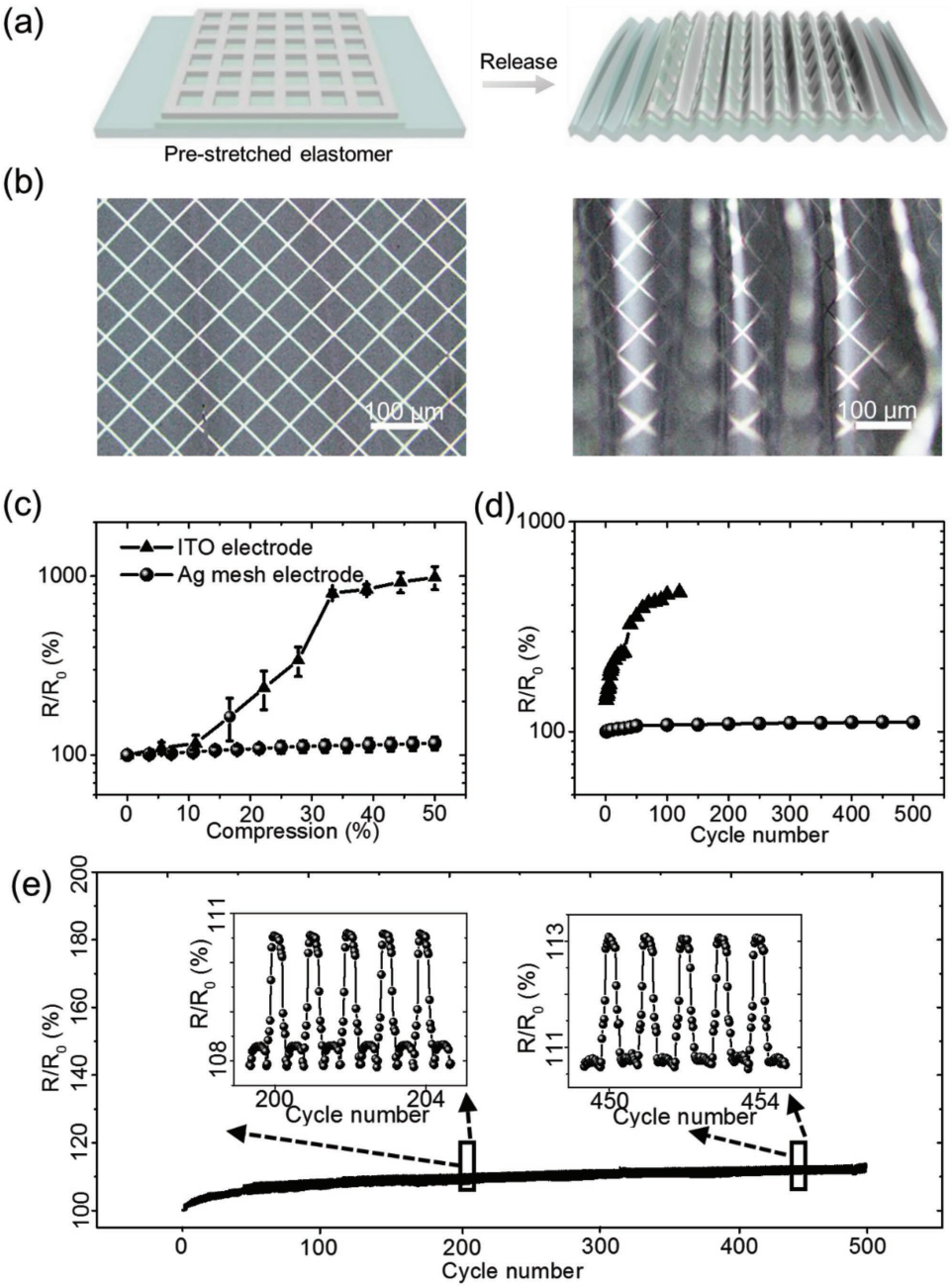

Figure 3. Mechanical test of ultrathin Ag mesh transparent electrodes. a) Schematic of compression-induced bending test. b) Optical images of Ag mesh transparent electrodes under 0% and 50% compression, showing an excellent conformability with a buckling structure. c,d) Increase in R_{sh} (c) under a series of compression and (d) after cycles at 100% stretch/release process for Ag mesh transparent electrodes and ITO electrodes with the same thickness on polyimide. e) Real-time recording of resistance change for Ag mesh transparent electrodes during cycling process.

smaller J_{SC} was caused by the loss of electrons during their collection when space length became larger. In contrast, the V_{OC} and FF were found to be relatively independent of the change in space length.

Figure 4f and Table S3 in the Supporting Information show a comparison between our Ag mesh OPV devices, with a space length of 45 μm, and sputtered ITO OPVs. Our devices showed an average PCE of 8.3%, J_{SC} of 16.83 mA cm^{-2}, V_{OC} of 0.85 V, and an FF of 0.58 under 100 mW cm^{-2} AM 1.5G illumination with negligible hysteresis. On the other hand, the sputtered ITO OPV devices had an average PCE of 8.5%, J_{SC} of 16.67 mA cm^{-2}, V_{OC} of 0.85 V, and an FF of 0.60. The corresponding comparison of external quantum efficiency (EQE) spectra can be seen in Figure S15 in the Supporting Information. The slight decrease in PCE is mainly caused by a smaller FF due to the lowered transmittance than ITO and micro-sized gaps in the Ag mesh electrodes. Further downscaling of the printing resolution via a smaller line width and space length is believed to enhance the

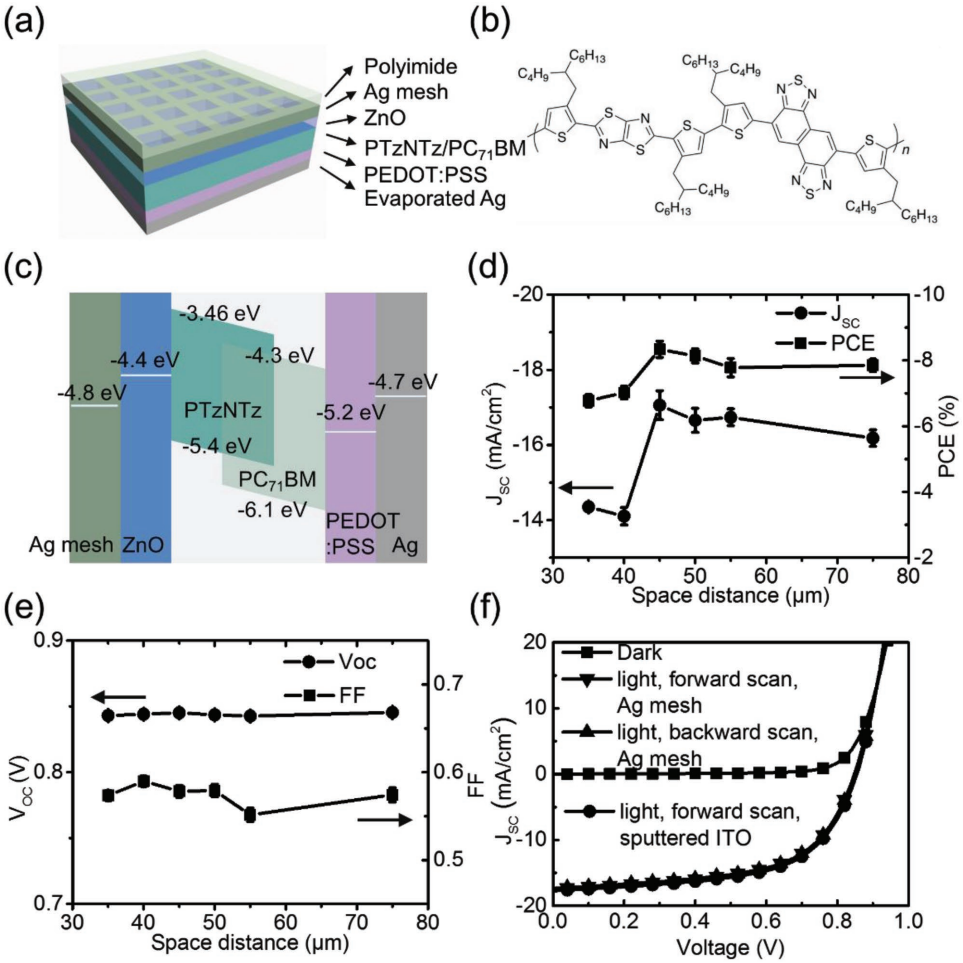

Figure 4. Ultrathin OPVs based on Ag mesh transparent electrodes. a) Structure of ultrathin OPVs. b) Chemical structure of PTzNTz. c) The corresponding energy-level diagram of each layer. d,e) Comparisons among (d) J_{SC} and PCE, (e) and V_{OC} and FF of different Ag mesh transparent electrodes, showing suitable space length should be between 45 and 50 μm. f) A comparison between *J*–*V* curves of OPVs based on Ag mesh and sputtered ITO transparent electrodes, where the space length of Ag mesh electrodes was 45 μm.

performance of Ag mesh based OPVs. For the case of Ag mesh electrodes, a common concern is whether it can properly function in an OPV. In Figure S14b in the Supporting Information, we provide a *J*–*V* curve of an OPV without light irradiation, where the leakage current was very small. Furthermore, the J_{SC} demonstrated a good linear relationship with light intensity (Figure S14c, Supporting Information). Thus, our ultrathin OPV based on printed Ag mesh electrodes demonstrates its potential for use in future high-performance and large-area renewable energy sources.

One of the most critical bottlenecks that limit mechanical durability of flexible photonic devices is the brittleness of ITO. In this work, we have succeeded in improving significantly the durability of transparent electrodes by replacing ITO with printed silver mesh electrodes. However, the organic photonic devices including organic photovoltaics have multilayered structures and, therefore, their mechanical durability is determined not only by the brittleness of transparent electrodes, but also the durability of other layers as well as interfacial properties such as adhesion between each layer. This is an important research direction for further improvement of the mechanical robustness of flexible organic ITO-free photonic devices.

In conclusion, we developed a reverse-offset printing process to print a uniform and ultrathin Ag mesh (100 nm) on ultraflexible substrates at a high speed (112.5 mm min^{-1} in the plane direction); the process is high throughput, cost-efficient, and roll-to-roll compatible. These Ag mesh transparent electrodes are lightweight, conformal, ultrastretchable, and mechanically durable. The conductance and transparency of Ag mesh transparent electrodes were tuned by the space length, and a 17 Ω sq^{-1} R_{sh} at 93.2% transmittance was achieved, which surpassed the performance of sputtered ITO electrodes and other ultrathin Ag mesh transparent electrodes. They also exhibited superior mechanical stability, with a buckling structure, displaying only a 16.6% increase in R_{sh} under 50% compression and a 10.6% increase in R_{sh} after 500 stretch/release strain cycles. To demonstrate their feasibility for high-performance ITO-free optoelectronic devices, Ag mesh transparent electrodes were applied in ultrathin OPVs. The optimized OPVs had a PCE of 8.3%, which is one of the most efficient OPVs ever reported using Ag mesh transparent electrodes.

Supporting Information

Supporting Information is available from the Wiley Online Library or from the author.

Acknowledgements

This work was financially supported by the JST PRESTO (Grant No. JPMJPR1428). The authors would like to thank Dr. D. D. Ordinario, Y. Jimbo, Y. Wu, H. Jinno, and R. Nur of The University of Tokyo (Japan) and H. Kimura of Center for Emergent Matter Science in RIKEN for their technical support and helpful discussions. The authors also appreciate R. Nur of The University of Tokyo (Japan) for editing and proofreading the manuscript. Z.J. is supported by JRA program in RIKEN and SRUT RA program in the University of Tokyo.

Conflict of Interest

K. Fukuda was a consultant for DIC Corporation. Ag ink (RAGT) was provided from DIC Corporation without any charge.

Keywords

Ag mesh, mechanical robustness, reverse-offset printing, stretchable transparent electrodes, ultrathin photonic devices

Received: December 25, 2017
Revised: March 10, 2018
Published online: May 7, 2018

[1] S. H. Shin, S. Ji, S. Choi, K. H. Pyo, B. Wan An, J. Park, J. Kim, J. Y. Kim, K. S. Lee, S. Y. Kwon, J. Heo, B. G. Park, J. U. Park, *Nat. Commun.* **2017**, *8*, 14950.
[2] T. Yokota, P. Zalar, M. Kaltenbrunner, H. Jinno, N. Matsuhisa, H. Kitanosako, Y. Tachibana, W. Yukita, M. Koizumi, T. Someys, *Sci. Adv.* **2016**, *2*, e1501856.
[3] V. Vohra, K. Kawashima, T. Kakara, T. Koganezawa, I. Osaka, K. Takimiya, H. Murata, *Nat. Photonics* **2015**, *9*, 403.
[4] T. Kim, J. H. Kim, T. E. Kang, C. Lee, H. Kang, M. Shin, C. Wang, B. Ma, U. Jeong, T. S. Kim, B. J. Kim, *Nat. Commun.* **2015**, *6*, 8547.
[5] A. Miyamoto, S. Lee, N. F. Cooray, S. Lee, M. Mori, N. Matsuhisa, H. Jin, L. Yoda, T. Yokota, A. Itoh, M. Sekino, H. Kawasaki, T. Ebihara, M. Amagai, T. Someya, *Nat. Nanotechnol.* **2017**, *12*, 907.
[6] N. Matsuhisa, D. Inoue, P. Zalar, H. Jin, Y. Matsuba, A. Itoh, T. Yokota, D. Hashizume, T. Someya, *Nat. Mater.* **2017**, *16*, 834.
[7] M. S. White, M. Kaltenbrunner, E. D. Głowacki, K. Gutnichenko, G. Kettlgruber, I. Graz, S. Aazou, C. Ulbricht, D. A. M. Egbe, M. C. Miron, Z. Major, M. C. Scharber, T. Sekitani, T. Someya, S. Bauer, N. S. Sariciftci, *Nat. Photonics* **2013**, *7*, 811.
[8] H. Jinno, K. Fukuda, X. Xu, S. Park, Y. Suzuki, M. Koizumi, T. Yokota, I. Osaka, K. Takimiya, T. Someya, *Nat. Energy* **2017**, *2*, 780.
[9] D. S. Hecht, L. Hu, G. Irvin, *Adv. Mater.* **2011**, *23*, 1482.
[10] P. C. Hsu, S. Wang, H. Wu, V. K. Narasimhan, D. Kong, H. Ryoung Lee, Y. Cui, *Nat. Commun.* **2013**, *4*, 2522.
[11] J. Jiu, M. Nogi, T. Sugahara, T. Tokuno, T. Araki, N. Komoda, K. Suganuma, H. Uchida, K. Shinozaki, *J. Mater. Chem.* **2012**, *22*, 23561.
[12] Y. Yang, S. Ding, T. Araki, J. Jiu, T. Sugahara, J. Wang, J. Vanfleteren, T. Sekitani, K. Suganuma, *Nano Res.* **2016**, *9*, 401.
[13] J. Lee, J. Y. Woo, J. T. Kim, B. Y. Lee, C. S. Han, *ACS Appl. Mater. Interfaces* **2014**, *6*, 10974.
[14] C. F. Guo, Q. Liu, G. Wang, Y. Wang, Z. Shi, Z. Suo, C. W. Chu, Z. Ren, *Proc. Natl. Acad. Sci. USA* **2015**, *112*, 12332.
[15] T. Sekitani, H. Nakajima, H. Maeda, T. Fukushima, T. Aida, K. Hata, T. Someya, *Nat. Mater.* **2009**, *8*, 494.
[16] S. Bae, H. Kim, Y. Lee, X. Xu, J. S. Park, Y. Zheng, J. Balakrishnan, T. Lei, H. R. Kim, Y. I. Song, Y. J. Kim, K. S. Kim, B. Ozyilmaz, J. H. Ahn, B. H. Hong, S. Iijima, *Nat. Nanotechnol.* **2010**, *5*, 574.
[17] J. L. Xu, Y. H. Liu, X. Gao, Y. Sun, S. Shen, X. Cai, L. Chen, S. D. Wang, *ACS Appl. Mater. Interfaces* **2017**, *9*, 27649.
[18] T. Yamada, K. Fukuhara, K. Matsuoka, H. Minemawari, J. Tsutsumi, N. Fukuda, K. Aoshima, S. Arai, Y. Makita, H. Kubo, T. Enomoto, T. Togashi, M. Kurihara, T. Hasegawa, *Nat. Commun.* **2016**, *7*, 11402.
[19] Z. Zhang, X. Zhang, Z. Xin, M. Deng, Y. Wen, Y. Song, *Adv. Mater.* **2013**, *25*, 6714.
[20] C.-J. Moon, I. Kim, S.-J. Joo, W.-H. Chung, T.-M. Lee, H.-S. Kim, *Thin Solid Films* **2017**, *629*, 60.
[21] L. Kinner, S. Nau, K. Popovic, S. Sax, I. Burgués-Ceballos, F. Hermerschmidt, A. Lange, C. Boeffel, S. A. Choulis, E. J. W. List-Kratochvil, *Appl. Phys. Lett.* **2017**, *110*, 101107.
[22] J. van de Groep, P. Spinelli, A. Polman, *Nano Lett.* **2012**, *12*, 3138.
[23] M.-G. Kang, M.-S. Kim, J. Kim, L. J. Guo, *Adv. Mater.* **2008**, *20*, 4408.
[24] S. Hong, J. Yeo, G. Kim, D. Kim, H. Lee, J. Kwon, Y. Lee, P. Lee, S.-H. Ko, *ACS Nano* **2013**, *7*, 5024.
[25] M. Helgesen, J. E. Carlé, F. C. Krebs, *Adv. Energy Mater.* **2013**, *3*, 1664.
[26] Y. Jang, J. Kim, D. Byun, *J. Phys. D: Appl. Phys.* **2013**, *46*, 155103.
[27] H. Wu, D. Kong, Z. Ruan, P. C. Hsu, S. Wang, Z. Yu, T. J. Carney, L. Hu, S. Fan, Y. Cui, *Nat. Nanotechnol.* **2013**, *8*, 421.
[28] E. C. Garnett, W. Cai, J. J. Cha, F. Mahmood, S. T. Connor, M. G. Christoforo, Y. Cui, M. D. McGehee, M. L. Brongersma, *Nat. Mater.* **2012**, *11*, 241.
[29] D. Angmo, T. T. Larsen-Olsen, M. Jørgensen, R. R. Søndergaard, F. C. Krebs, *Adv. Energy Mater.* **2013**, *3*, 172.
[30] F. C. Krebs, *Org. Electron.* **2009**, *10*, 761.
[31] J. A. Farmer, C. T. Campbell, *Science* **2010**, *329*, 933.
[32] Y. Leterrier, L. Médico, F. Demarco, J. A. E. Månson, U. Betz, M. F. Escolà, M. Kharrazi Olsson, F. Atamny, *Thin Solid Films* **2004**, *460*, 156.
[33] M. Wang, J. Wang, W. Chen, Y. Cui, L. Wang, *Mater. Chem. Phys.* **2006**, *97*, 219.
[34] S. K. Lin, S. Nagao, E. Yokoi, C. Oh, H. Zhang, Y. C. Liu, S. G. Lin, K. Suganuma, *Sci. Rep.* **2016**, *6*, 34769.
[35] J. H. Lee, D. Y. Youn, Z. Luo, J. Y. Moon, S. J. Choi, C. Kim, I. D. Kim, *ACS Appl. Mater. Interfaces* **2017**, *9*, 39650.
[36] S. Jeong, H. C. Song, W. W. Lee, Y. Choi, S. S. Lee, B. H. Ryu, *J. Mater. Chem. C* **2010**, *114*, 22277.
[37] M. Saito, I. Osaka, Y. Suzuki, K. Takimiya, T. Okabe, S. Ikeda, T. Asano, *Sci. Rep.* **2015**, *5*, 14202.